

Dynamical Origin of (469219) Kamo‘oalewa of Tianwen-2 Mission from the Main-Belt: ν_6 Secular Resonance, Flora Family or 3:1 Resonance with Jupiter

Yandong Wang^{1,2}, Shoucun Hu^{1,2}, Jianghui Ji^{1,2} and Jiajun Ying^{1,2}

¹ Purple Mountain Observatory, Chinese Academy of Sciences, Nanjing 210023, China; jjh@pmo.ac.cn

² School of Astronomy and Space Science, University of Science and Technology of China, Hefei 230026, China

Received 202x month day; accepted 202x month day

Abstract China’s *Tianwen-2* mission, launched on 29 May 2025, targets the near-Earth object (469219) Kamo‘oalewa, an Earth quasi-satellite trapped in a 1:1 mean-motion resonance with our planet. Determining the origin of Kamo‘oalewa is central to understanding the formation pathways and dynamical evolution of Earth’s quasi-satellite population. Here we show a strong possibility of main-belt origin for Kamo‘oalewa using long-term dynamical simulations. We examine three candidate source regions: the ν_6 secular resonance (ν_6), the 3:1 mean-motion resonance with Jupiter (3:1J MMR), and the Flora family. A total of 42 825 test particles were integrated over 100 Myr. We find that asteroids from all three regions can be transported onto Kamo‘oalewa-like orbits, albeit with markedly different efficiencies. Particles originating near the ν_6 show the highest transfer probability (3.31%), followed by the Flora family (2.54%) and the 3:1J MMR (0.39%). We further identify representative dynamical pathways linking these source regions to Earth quasi-satellite orbits. The *Tianwen-2* spacecraft is expected to rendezvous with Kamo‘oalewa in 2026, performing close-proximity operations and returning samples. The mission will provide decisive observational constraints on the asteroid’s composition and physical properties, offering a critical test of its proposed origin.

Key words: minor planets, asteroids: individual: (469219) Kamo‘oalewa — celestial mechanics — methods: numerical

1 INTRODUCTION

China’s *Tianwen-2* mission is designed to advance the exploration of small bodies by conducting rendezvous and sample-return operations at a near-Earth asteroid. Launched on 2025 May 29, the spacecraft

targets (469219) Kamo‘oalewa (provisional designation 2016 HO₃), discovered on 2016 April 27 by the Pan-STARRS1 survey telescope at the Haleakala Observatory in Hawaii, which is known as an Earth quasi-satellite temporarily trapped in a 1:1 mean-motion resonance with Earth (de la Fuente Marcos & de la Fuente Marcos 2016). Such objects provide a natural laboratory for studying the dynamical coupling between the near-Earth population and the main-belt. Through close-proximity observations and the return of pristine material, *Tianwen-2* will place new constraints on the physical properties and origin of quasi-satellites.

In the restricted three-body problem, quasi-satellites (also referred to as retrograde satellites; Jackson 1913) constitute a special class of small bodies locked in 1:1 mean-motion resonance with their host planet, with the relative mean longitude librating around 0°(de la Fuente Marcos & de la Fuente Marcos 2016). In a heliocentric frame of reference that rotates with host planet, these objects exhibit satellite-like apparent motion, orbiting the planet; however, their orbits always remain outside the radius of the Hill sphere of the host planet and they are not gravitationally bound. Dynamically, they therefore retain heliocentric orbits rather than true satellite states (Mikkola et al. 2006). As of November 2025, only 8 Earth quasi-satellites have been confirmed, among which (469219) Kamo‘oalewa is one of the most dynamically stable Earth co-orbitals currently known (de la Fuente Marcos & de la Fuente Marcos 2016, 2025). Its distinctive physical and dynamical properties make it an important target for studies of Earth co-orbitals.

Kamo‘oalewa has an absolute magnitude $H = 24.33$ mag and a semimajor axis $a = 1.00098$ au (at epoch JD 2461000.5), yielding an orbital period very close to that of Earth. Its orbital eccentricity and inclination are $e = 0.10237$ and $i = 7.80322^\circ$, respectively. Broadband color photometry and visible spectra indicate that its taxonomic class is consistent with S-type silicate asteroids, but with a redder spectral slope than typical S-type objects (Sharkey et al. 2021), suggesting that it may have experienced substantial space weathering (Zhang et al. 2024). Assuming a geometric albedo of 0.1, Zhang et al. (2024) estimated an equivalent diameter of approximately 57 m. In addition, Kamo‘oalewa exhibits an exceptionally rapid rotation period of about 28 min, well below the 2.2-h spin barrier for cohesionless small bodies (Pravec & Harris 2000; Chang et al. 2017). This implies that it may possess a relatively coherent monolithic interior, possibly mantled by a regolith layer composed of millimeter- to centimeter-sized particles (Li & Scheeres 2021; Cheng & Baoyin 2024; Liu et al. 2024; Ren et al. 2024; Ying et al. 2025).

From a dynamical perspective, numerical simulations by de la Fuente Marcos & de la Fuente Marcos (2016) showed that Kamo‘oalewa undergoes recurrent and stable transitions between the quasi-satellite and horseshoe configurations on Myr timescales. Its current quasi-satellite phase is estimated to have begun about 100 yr ago and is expected to end in roughly 300 yr. Furthermore, Fenucci & Novaković (2021) explored the long-term dynamical consequences of Yarkovsky-induced semimajor-axis drift for Kamo‘oalewa under different surface thermal-property scenarios. They showed that while the Yarkovsky effect has little influence on the short-term dynamics of the asteroid, it can significantly affect its long-term stability for low surface thermal conductivity, accelerating its escape from the Earth co-orbital region. Building on this theoretical framework, Liu et al. (2022) reported the first observational detection of the Yarkovsky effect acting on Kamo‘oalewa based on ground-based optical astrometry. Their results confirmed that the effect is negligible on short timescales but reduces the asteroid’s residence time in the Earth co-orbital state, in agreement with earlier numerical predictions. Further advances were made by Hu et al. (2023), who derived

new estimates of the non-gravitational parameter A_2 and explored the propagation of orbital instability, suggesting that the quasi-satellite configuration itself may play a key role in limiting orbital uncertainty. Using updated astrometric observations, Fenucci et al. (2025) further constrained the non-gravitational parameter A_2 and the thermal inertia of Kamo‘oalewa, thereby improving the predicted targeting accuracy of the *Tianwen-2* spacecraft during its encounter.

Unlike long-lived co-orbital populations such as the Jovian Trojans, the complex multi-body perturbations in the inner Solar System lead to a much higher degree of orbital chaos for NEOs (Morais & Morbidelli 2002). As a result, co-orbital small bodies associated with terrestrial planets exhibit rich and distinctive dynamical behaviors, and their origins and evolutionary pathways provide important insights onto the dynamical structure of the inner Solar System.

Recently, the origin of Kamo‘oalewa has been the subject of several dedicated studies. Based on analysis of visible and near-infrared reflectance spectral, Sharkey et al. (2021) found that the spectral characteristics of this object, particularly the position and shape of the $1\text{ }\mu\text{m}$ absorption band, are highly similar to those of lunar regolith samples returned by the Apollo mission, and for the first time proposed a lunar-origin hypothesis for Kamo‘oalewa.

Using N -body numerical simulations, Castro-Cisneros et al. (2023) examined the dynamical feasibility of lunar impact ejecta being injected into the Earth co-orbital region. They showed that lunar ejecta released from the trailing side of the Moon at velocities slightly exceeding the lunar escape speed have a non-negligible probability of being captured as Earth co-orbital objects, and may even evolve into quasi-satellite orbits. Combining spectral constraints with dynamical analyses, Jiao et al. (2024) argued that Kamo‘oalewa most likely originated from the young lunar impact crater Giordano Bruno. In contrast, Zhu et al. (2025) based on more detailed spectral comparisons and impact-dynamical simulations, suggested that the Tycho crater may represent a source region more consistent with both observational and dynamical constraints.

Although previous studies have provided evidence supporting a lunar origin for Kamo‘oalewa from both spectroscopic observations and N -body numerical simulations, this scenario remains debated. Based on spectral analyses, Fenucci & Novaković (2021) were among the first to suggest that Kamo‘oalewa may be related to Barbarian asteroids in the main-belt and could have migrated to its current orbit through the 3:1J MMR, located at approximately 2.5 au, which corresponds to the commensurability $n/n_J = 3$, where n and n_J are the mean motions of the asteroid and Jupiter, respectively (Wisdom 1985; Gladman et al. 1997; Bottke et al. 2002; Granvik et al. 2018). Using spectral comparisons combined with orbital dynamical calculational method, Zhang et al. (2024) argued that Kamo‘oalewa is compositionally more consistent with LL chondrites and has a $72 \pm 5\%$ probability of originating from the ν_6 region, where the precession frequency of the asteroid’s longitude of perihelion g is equal to mean precession frequency of Saturn’s longitude of perihelion g_6 (Froeschle & Scholl 1989; Morbidelli et al. 2002). The main-belt, particularly its strong resonant regions, is widely regarded as the primary source of NEOs (Binzel et al. 1992; Morbidelli et al. 2002; Morbidelli & Vokrouhlický 2003; Michel et al. 2005). In this context, Earth co-orbital objects do not constitute an isolated dynamical population but may be connected with near-Earth and main-belt asteroids. It is therefore necessary to assess the dynamical feasibility of main-belt regions producing Kamo‘oalewa-like orbital configurations.

In addition, existing dynamical simulations investigating a lunar origin for Kamo‘oalewa have considered only planetary gravitational perturbations and have not incorporated the Yarkovsky effect. For small bodies with diameters of only several tens of meters, this effect can significantly modify orbital evolution on Myr timescales, thereby altering the probability of entering and maintaining co-orbital configurations (Fenucci & Novaković 2021; Liu et al. 2022). These limitations leave substantial room for further investigation of the origin and dynamical evolution of Kamo‘oalewa from a dynamical perspective.

Motivated by this, we use numerical integrations that include Yarkovsky-driven forces to assess whether Kamo‘oalewa could originate from the main-belt and to identify the dynamical pathways by which particles evolve onto Kamo‘oalewa-like orbits. The *Tianwen-2* spacecraft is scheduled to rendezvous with Kamo‘oalewa in July 2026, marking China’s first asteroid sample-return mission, and our results provide essential dynamical context for interpreting the mission’s forthcoming observations.

This paper is organized as follow: Section 2 introduces the data and the numerical setup in this study. Section 3 analysis the results and presents several representative evolutionary paths for our candidate sources. The conclusion and discussions are presented in Section 4.

2 DATA AND METHOD

de la Fuente Marcos & de la Fuente Marcos (2016) reported that the Lyapunov time of Kamo‘oalewa is approximately 7500 yr, indicating a high degree of orbital chaos on relatively short timescales. Moreover, (Morbidelli et al. 2020) pointed out that long-term backward orbital integrations cannot reliably trace the origin of small bodies. In light of these considerations, we adopt a forward orbital integrations approach combined with statistical analysis to assess the dynamical feasibility of objects from different main-belt sources evolving toward the current orbit of Kamo‘oalewa. Our focus is on the statistical behavior of test particles, under the assumption that, for sufficiently large samples, the collective evolution of a large number of test particles can provide a representative picture of the likely dynamical pathways leading to Kamo‘oalewa.

Based on the debiased NEOs model proposed by Nesvorný et al. (2024), we estimated the potential dynamical sources of Kamo‘oalewa. The results indicate that the ν_6 and 3:1J MMR (Ji & Liu 2007; Nesvorný et al. 2023) in the main-belt are the most probable contributors, with corresponding probabilities of 71.7% and 17.5%, respectively. In addition, Zhang et al. (2024) further suggested that the Flora family also warrants consideration. Flora family corresponds to a major asteroid family in the inner main-belt located near ν_6 and is considered a primary source of LL chondrite-like NEOs as well as Earth–Moon impactors (Vokrouhlický et al. 2017; Zhang et al. 2025a). Considering the above factors, we select three candidate sources in the main-belt, namely the ν_6 , the 3:1J MMR, and the Flora family, for further numerical simulations to investigate the dynamical origin of such orbits.

The approximate boundaries of ν_6 and 3:1J MMR are defined following the method of Nesvorný et al. (2023), with Mars-crossing objects excluded. In view of the phase-space structure of the ν_6 in the vicinity of the 3:1J MMR, we restrict the upper inclination limit of ν_6 to 17°. Members of Flora family are obtained from the NASA Planetary Data System¹ (see also Nesvorný 2020).

¹ <https://sbn.psi.edu/pds/resource/nesvornymam.html>

We select real asteroids located in the three candidate sources from the MPCORB.DAT catalog provided by the Minor Planet Center (version dated 2025 June 04) and use them as simulated particles. The initial orbital elements of all simulated particles are taken directly from this catalog, with an initial epoch of JD 2460800.5.

It should be emphasized that our numerical simulations are not intended to investigate the detailed evolution of individual real asteroids. Instead, the observed asteroids are treated as samples of the corresponding sources, allowing us to extract statistically representative dynamical behaviors and underlying mechanisms in their long-term evolution.

The total number of sampled particles is 42 825, including 7 122 in the ν_6 , 13 786 in the Flora family, and 21 917 in the 3:1J MMR. The initial distribution of these particles in the $a-i$ plane is shown in Fig. 1.

We perform numerical integrations of the simulated particles using the Hybrid integrator of the MERCURY6 package (Chambers 1999). Gravitational perturbations from all big bodies from Mercury to Pluto are included, while the Earth–Moon system is represented by its barycenter. The initial states of all perturbing bodies are taken from the JPL Ephemerides DE441 (Park et al. 2021) and are set at the same epoch as the simulated particles.

The codes are modified to incorporate the Yarkovsky effect in this work. Although the acceleration induced by the Yarkovsky effect is much smaller than that due to planetary gravitational perturbations, it can lead to long-term variations in the semimajor axis a by increasing or decreasing the orbital energy of small bodies on timescales of Myr to Gyr (Bottke et al. 2006; Vokrouhlicky et al. 2015). A precise treatment of the Yarkovsky effect requires detailed knowledge of the physical properties of individual objects; however, given the limited constraints on the physical properties of Kamo‘oalewa, we adopt a simplified Yarkovsky acceleration model following Deo & Kushvah (2017) and Hu et al. (2023):

$$\mathbf{F}_{\text{Yark}} = A_2 (r_0/r)^d \hat{\mathbf{t}} \quad (1)$$

where $r_0 = 1$ au is a reference heliocentric distance, r is the instantaneous heliocentric distance of the particle expressed in au, and d is a parameter related to the thermophysical properties of the asteroid. In this work, we adopt $d = 2$. The unit vector $\hat{\mathbf{t}}$ points in the transverse direction of the orbit, and A_2 is the non-gravitational transverse parameter, taken from the value reported by the JPL Horizons system for Kamo‘oalewa, $A_2 = -1.3455 \times 10^{-13}$ au day $^{-2}$, corresponding to a retrograde rotation state, and is held constant throughout the integrations. We adopt a single, fixed value of A_2 , applied uniformly to all test particles in our simulations for Kamo‘oalewa.

During the integrations, all simulated particles are treated as massless bodies and are subject only to gravitational perturbations from the massive bodies and the Yarkovsky effect. A simulated particle is removed from the integrations if it collides with any massive body or if its heliocentric distance exceeds 100 au.

Following the approach of Bottke et al. (2015), we apply a modified criterion to identify particles that evolve onto Kamo‘oalewa-like orbits. Specifically, we compute the mean orbital elements $(\bar{a}, \bar{e}, \bar{i})$ of Kamo‘oalewa over a time interval of 2×10^4 yr, yielding $(0.99989 \text{ au}, 0.09934, 7.57547^\circ)$. This criterion is designed to reduce the influence of short-term fluctuations in the osculating orbital elements on the classification. A simulated particle is classified as Kamo‘oalewa-like if its evolving orbital elements satisfy

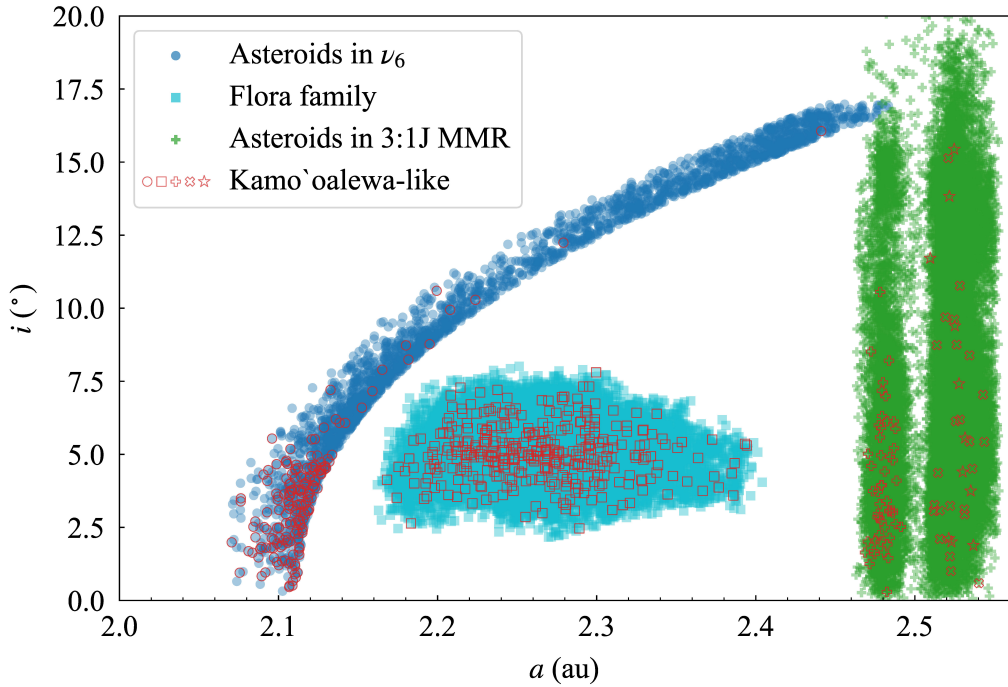


Fig. 1: Initial distribution of simulated particles in the a – i plane. Blue circles, cyan squares, and green plus symbols denote particles initially located near the ν_6 , the Flora family, and the 3:1J MMR, respectively. Red open symbols indicate particles from the candidate sources that eventually evolve onto Kamo‘oalewa-like orbits during the integrations. For particles initially associated with the 3:1J MMR, red open plus and cross symbols represent those evolving onto Kamo‘oalewa-like orbits via the ν_6 and 3:1J MMR, respectively, while red star symbols denote particles that first cross the 3:1J MMR and subsequently evolve via the ν_6 .

$\Delta a \leq 0.01$ au, $\Delta e \leq 0.1$, and $\Delta i \leq 5^\circ$, where Δa , Δe , and Δi denote the absolute differences from the reference mean values. Although the adopted criteria are broader than those used in previous studies (e.g., Bottke et al. 2015; Zhou et al. 2019), given that Kamo‘oalewa undergoes transitions among different co-orbital states, its orbital elements can vary over a relatively broad range with time (de la Fuente Marcos & de la Fuente Marcos 2016). Accordingly, we adopt a relatively wide set of criteria to encompass the temporal variability of its orbital elements over a finite interval, rather than to match only its instantaneous present-day orbit. Our aim is not to reproduce the exact current quasi-satellite configuration of Kamo‘oalewa, but to identify simulated particles whose orbital evolution is comparable to that of Kamo‘oalewa over a certain timescale.

3 RESULTS

After including the Yarkovsky effect, we integrated a total of 42 825 real asteroids selected from three candidate main-belt sources: the ν_6 , the 3:1J MMR, and the Flora family for a duration of 100 Myr. We then identified particles that escape from these regions and subsequently evolve onto Kamo‘oalewa-like orbits.

In total, 672 simulated particles from the three candidate sources are found to reach Kamo‘oalewa-like orbits during the integrations. Among them, 236 originate from the ν_6 , 350 from the Flora family, and 86 from the 3:1J MMR, corresponding to fractions of 3.31%, 2.54% and 0.39% of their respective source

populations. These results indicate that, although Kamo‘oalewa-like orbits occupy only a limited region in the present-day phase space, particles originating from the main-belt can still reach such configurations.

The distribution of Kamo‘oalewa-like particles in initial orbital-parameter space shows additional features. Among particles originating from the ν_6 , about 96.2% are found at inclinations lower than 7.8° (the present inclination of Kamo‘oalewa), whereas the corresponding fraction for the 3:1J MMR is about 83.7%. This distribution indicates that, for the two dynamical source regions considered here, only particles with specific initial orbital parameters in phase space—particularly those with lower initial inclinations—are able to evolve onto Kamo‘oalewa-like orbits.

During their dynamical evolution, simulated particles exhibit relatively regular orbital behavior while residing in the main-belt, but become increasingly chaotic after entering the near-Earth region (Fig. 2). Overall, their evolution is governed by a combination of gravitational scattering by the massive bodies and episodes of temporary resonance capture, primarily involving two-body and three-body mean-motion resonances with Earth, Mars, and Jupiter. This general evolutionary behavior is consistent with the results reported by Gladman et al. (1997) and Michel et al. (2005).

Fig. 2 illustrates the representative evolutionary behaviors of particles originating from the three candidate sources. In general, particles spend most of their evolutionary lifetimes in the main-belt during their migration toward the near-Earth region. Once they approach the main-belt escape channels—dominated in our simulations by the ν_6 and the 3:1J MMR—they reach the near-Earth region on timescales of 10^5 – 10^6 yr.

Panel A of Fig. 2 shows a representative evolutionary pathway of a particle originating near the ν_6 . The particle initially resides at $a = 2.15$ au and $i = 5.8^\circ$ and is locked in the ν_6 with the resonant angle $\Delta\varpi = \varpi - \varpi_6$ oscillating around 180° , where ϖ and ϖ_6 denote the longitudes of perihelion of the particle and Saturn, respectively. This configuration corresponds to a relatively stable anti-aligned state with Saturn (Carruba et al. 2022), allowing the particle to remain in the ν_6 for approximately 12 Myr. During this stage, the eccentricity exhibits oscillatory behavior with a slow overall increase, remaining insufficient to reduce the perihelion distance to Earth-crossing values. Over the subsequent ~ 1 Myr, the eccentricity rapidly increases to ~ 0.6 , driving the particle into an Earth-crossing orbit and eventually causing it to escape from the resonance following a close encounter with Earth.

After leaving the resonance, the particle evolves while its perihelion remains near $q \simeq 1$. During this phase, it experiences multiple episodes of temporary resonance capture. As shown in the right panel of Fig. 2A, these resonances modulate not only the eccentricity but also the inclination, leading to oscillations in i while the a remains nearly constant. The capture durations range from a few thousand to several tens of thousands of years. The longest capture occurs near $a \simeq 1.524$ au, corresponding to a 1:1 mean-motion resonance with Mars (marked by a vertical dashed line), where the particle remains for nearly 3×10^4 yr and its inclination decreases from $\sim 8^\circ$ to $\sim 4^\circ$.

Because a negative value of the Yarkovsky parameter A_2 is adopted in the simulations, the semimajor axis of the particles exhibits a long-term inward drift (Farnocchia et al. 2013). As a result, particles initially located in the Flora family experience a gradual decrease in semimajor axis, causing their orbits to drift in a toward the characteristic semimajor axis of the ν_6 , as illustrated in Fig. 2B. After entering the ν_6 at ~ 30 Myr, the eccentricity is excited to ~ 0.4 within 3 Myr, allowing the particle to become Mars-crosser.

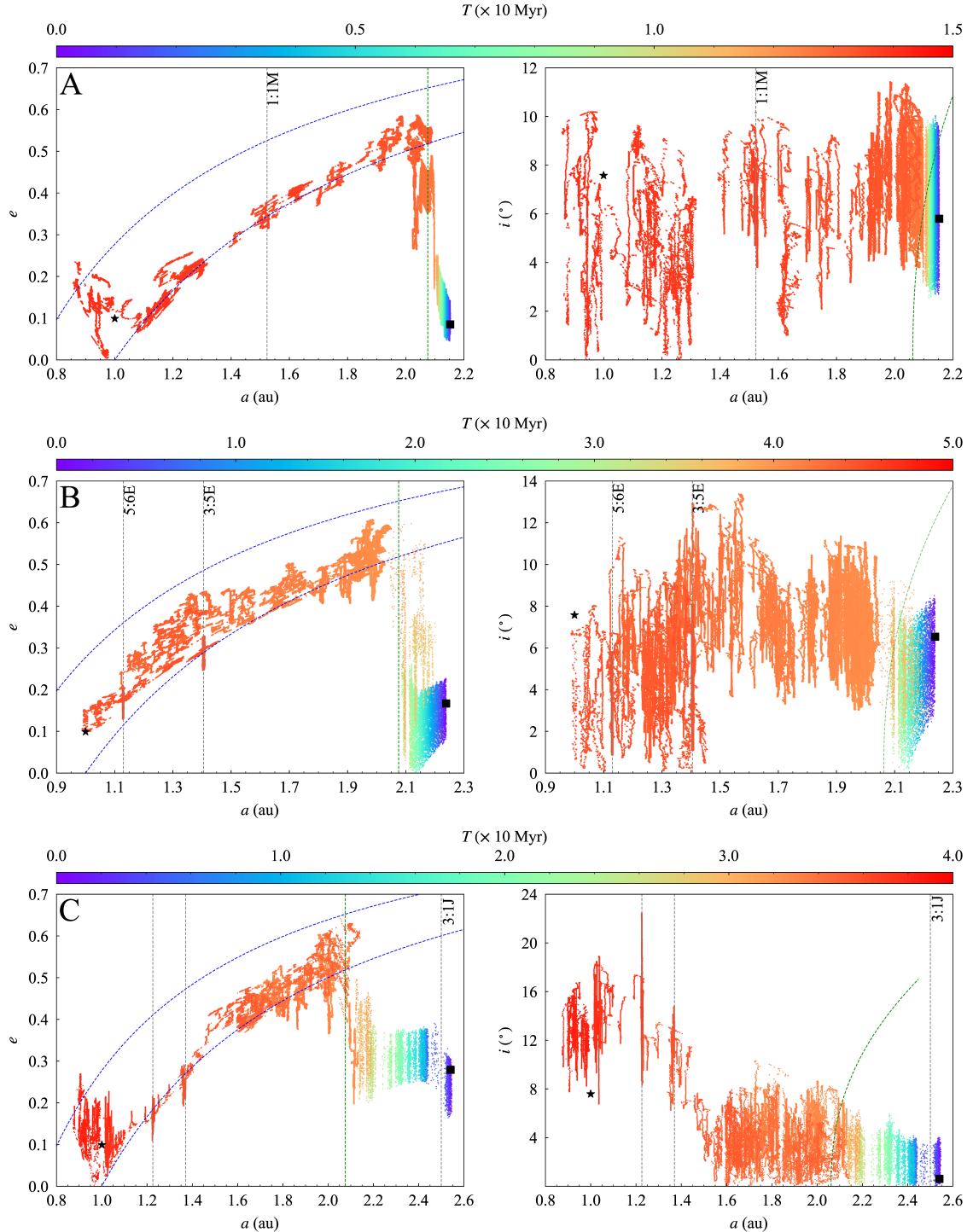


Fig. 2: From top to bottom, the A, B and C panels show the representative orbital evolutions of simulated particles from the ν_6 , the Flora family, and the 3:1J MMR, respectively, from the main-belt (time $T = 0$) to Kamō'oalewa-like orbits in the $a-e$ (left) and $a-i$ (right) planes. Colors indicate time progression from purple (early stages) to red (approaching Kamō'oalewa-like orbits). Black squares mark initial particle positions, and the black stars denote the current position of Kamō'oalewa. Gray dashed lines indicate representative mean-motion resonances, with unlabeled ones corresponding to closely spaced resonances. Green and blue dashed lines show the approximate location of the ν_6 and the loci where the perihelion distance equals that of the Earth or Venus, respectively. For clarity, the scattered points are shown after down-sampling.

Subsequent close encounters with Mars further drive the particle into an Earth-crossing orbit. The later evolution of this particle closely resembles that of particles initially located near the ν_6 . In Fig. 2B, vertical dashed lines mark several episodes of temporary resonance capture near $a \simeq 1.225$ au and $a \simeq 1.37$ au, where dense resonant structures delay the delivery of particle onto Kamo‘oalewa-like orbits.

The asteroids initially located near the 3:1J MMR exhibit more diverse behaviors owing to their distribution on both sides of the resonance (Fig. 1). Particles starting on the right-hand side of the resonance (marked by red open crosses) experience inward semimajor-axis drift driven by the Yarkovsky effect, as only a negative value of A_2 is adopted in our simulations. Given the strong efficiency of the 3:1J MMR in exciting eccentricities, particles entering the resonance have a much higher probability of reaching planet-crossing eccentricities than those remaining outside it. In our simulations, particles drifting into the 3:1J MMR from the right-hand side of the resonance typically experience rapid eccentricity growth, reaching values of $e \gtrsim 0.6$ within less than 1 Myr, thereby becoming Earth-crossers, consistent with the results of Morbidelli & Gladman (1998). In contrast, particles initially located on the left-hand side of the resonance (marked by red open plus symbols) evolve in a manner similar to those from the Flora family, but require substantially longer migration times typically at least 50 Myr in our simulations to reach the ν_6 .

We further identify a third evolutionary channel, in which some particles initially located at $a > 2.5$ au (marked by red open stars) are not stably captured by the 3:1J MMR but instead cross it rapidly within ~ 0.1 Myr. During the crossing, their eccentricities undergo modest oscillations with amplitudes of ~ 0.2 . In our simulations, 11 particles reaching Kamo‘oalewa-like orbits follow this pathway. This behavior indicates that resonance capture at the 3:1J MMR is not inevitable for particles approaching from the right-hand side, but instead depends on factors such as the migration rate and/or initial orbital configuration. Similar resonance-crossing processes have been invoked to explain the origin of V-type asteroids located outside the Vesta family by Folonier et al. (2014), suggesting a common underlying dynamical mechanism. The subsequent evolution of particles that cross the 3:1J MMR is similar to that of particles initially located in the Flora family, as well as particles on the left-hand side of this resonance, with representative examples shown in Fig. 2C. All these particles follow similar evolutionary pathways, reaching Kamo‘oalewa-like orbits via the ν_6 , as evidenced by the libration of $\Delta\varpi$.

Fig. 3 summarizes the time required for simulated particles originating from the three candidate sources to evolve onto Kamo‘oalewa-like orbits. The results show that during the early stage of the integrations (the first ~ 30 Myr), Kamo‘oalewa-like objects are predominantly supplied by particles initially located near the ν_6 , indicating that this region is more efficient at delivering particles onto Kamo‘oalewa-like orbits at early times.

As the integrations proceed, the relative contribution from the Flora family gradually increases and eventually becomes dominant. This transition can be attributed to the long-term action of the Yarkovsky effect, which continuously drives particles from the Flora family inward in semimajor axis, allowing them to progressively enter the ν_6 and thereby substantially enhancing their probability of evolving onto Kamo‘oalewa-like orbits.

In contrast, the time distribution near the 3:1J MMR exhibits a distinct pattern. As discussed above, particles contributing at shorter timescales mainly originate from the right-hand side of the 3:1J MMR and

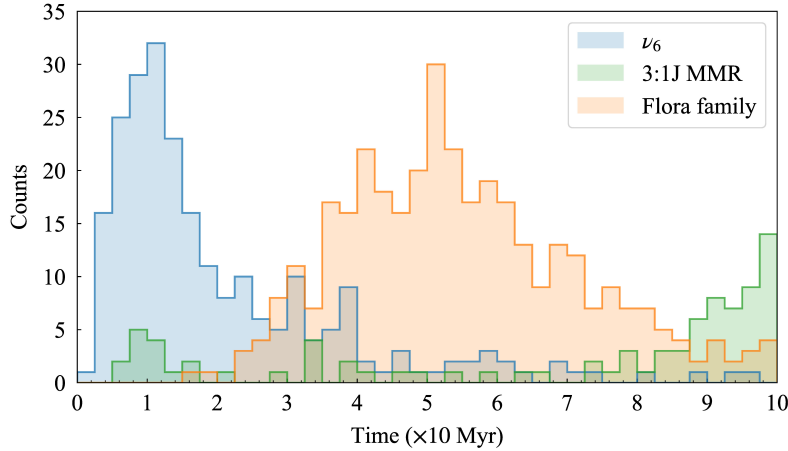


Fig. 3: Statistical distribution of the time required for simulated particles originating from the three candidate source regions to evolve from their initial locations into Kamo'alewa-like orbits.

evolve onto Kamo'alewa-like orbits after their eccentricities are directly excited during resonance interaction. In our simulations, about 50% of particles transported via the 3:1J MMR reach Kamo'alewa-like orbits within 20 Myr. The obvious increase appearing after 80 Myr in Fig. 3 is produced by a combination of particles initially located on the left-hand side of the resonance and particles originating on the right-hand side that undergo resonance crossing before evolving further.

Recent spectral analyses by Zhang et al. (2024) suggest that Kamo'alewa is a space-weathering-matured object, with a relevant timescale of at least ~ 50 Myr. In combination with our results shown in Fig. 3, Kamo'alewa-like objects show a preference for originating from the Flora family or the 3:1J MMR. Nevertheless, a contribution from the ν_6 source region cannot be completely ruled out.

Taken together, our results indicate that, given the established transport of main-belt objects into near-Earth space, main-belt regions can provide dynamically viable pathways leading to Kamo'alewa-like orbits. Although such evolutionary outcomes represent only a small fraction of the overall population, their existence demonstrates that the main-belt origin for Kamo'alewa-like objects is highly likely on dynamical grounds.

4 CONCLUSION AND DISCUSSIONS

Previous studies on the origin of (469219) Kamo'alewa have largely focused on a lunar impact-ejecta scenario, with significant insights gained from spectroscopic and dynamical analyses. Yet it remains unclear whether known near-Earth object reservoirs, particularly the main-belt, can dynamically supply Kamo'alewa-like objects to the near-Earth region. Here, we explore this possibility and investigate the main-belt pathways that could deliver such bodies. Incorporating the Yarkovsky effect, we carry out long-term numerical integrations with the MERCURY6 package for 42 825 asteroids drawn from three main-belt source regions: the ν_6 , the 3:1J MMR, and the Flora family. Our goal is to systematically assess whether the main-belt can dynamically supply objects onto Kamo'alewa-like orbits.

Our simulations show that a fraction of particles from the ν_6 , the 3:1J MMR, and the Flora family can evolve onto Kamo'alewa-like orbits, with transfer efficiencies of 3.31%, 0.39%, and 2.54%, respectively. These findings indicate that the main-belt, particularly the low-inclination inner region, can serve as a viable

source of Kamo‘oalewa-like objects. We further examine representative dynamical pathways: particles from the Flora family and near the ν_6 are mainly delivered via the ν_6 , whereas those near the 3:1J MMR follow more diverse routes, through either the 3:1J MMR or the ν_6 . We note that these pathways are illustrative and do not exhaust all possible evolutionary scenarios.

Overall, our results show that the Moon is not the only dynamically accessible source of Kamo‘oalewa (Jiao et al. 2024; Zhu et al. 2025). We identify representative transport pathways from main-belt candidate regions that deliver particles onto Kamo‘oalewa-like orbits. It should be noted that NEOs sources are distributed across the entire main-belt (e.g., Morbidelli et al. 2002; Granvik et al. 2017; Zhou et al. 2024, 2025). However, here we focus on dynamically efficient pathways/regions that are most relevant to producing Kamo‘oalewa. Within the adopted integration timescale of 100 Myr, classical strong resonances such as ν_6 and 3:1J MMR represent the most efficient routes for transporting main-belt bodies into the near-Earth region. As a first step, we therefore systematically examine a limited number of the most probable and efficient pathways relevant to the formation of Kamo‘oalewa-like orbits. Future work will address the transition from this orbital domain to the current co-orbital state of Kamo‘oalewa through more restrictive criteria and dedicated analysis.

Over the past decades, a number of asteroid exploration missions have significantly enhanced our understanding of small bodies through a combination of rendezvous, sample-return, and flyby observations. In addition to dedicated missions such as Hayabusa, Hayabusa2 and OSIRIS-REx, which explored the near-Earth asteroids like Itokawa, Ryugu, and Bennu (Fujiwara et al. 2006; Yano et al. 2006; Watanabe et al. 2017; Lauretta et al. 2017, 2019; Watanabe et al. 2019; Kitazato et al. 2019; Hamilton et al. 2019; Arakawa et al. 2020; Potiszil et al. 2023; Glavin et al. 2025), respectively, several spacecraft also have performed close flybys of small bodies, including the Chang‘e-2 flyby of Toutatis (Huang et al. 2013; Jiang et al. 2015 and references therein). In this context, as the first sample-return mission to explore a small, rapidly rotating asteroid, the *Tianwen-2* mission (Zhang et al. 2019, 2025b; Ying et al. 2025) is expected to provide valuable insights into surface environments, interior structure and dynamical properties.

Acknowledgements We sincerely thank the referee for the valuable comments and constructive suggestions that have improved the quality of the manuscript. This work is financially supported by the National Natural Science Foundation of China (grant Nos. 12561160085 and 12150009), and the Foundation of Minor Planets of the Purple Mountain Observatory. This research has made use of data provided by the International Astronomical Union’s Minor Planet Center.

References

- Arakawa, M., Saiki, T., Wada, K., & et al. 2020, *Science*, 368, 67 11
- Binzel, R. P., Xu, S., Bus, S. J., & Bowell, E. 1992, *Science*, 257, 779 3
- Bottke, Jr., W. F., Vokrouhlický, D., Rubincam, D. P., & Nesvorný, D. 2006, *Annual Review of Earth and Planetary Sciences*, 34, 157 5
- Bottke, W. F., Morbidelli, A., Jedicke, R., et al. 2002, *Icarus*, 156, 399 3
- Bottke, W. F., Vokrouhlický, D., Walsh, K. J., et al. 2015, *Icarus*, 247, 191 5, 6
- Carruba, V., Aljbaae, S., Domingos, R. C., Huaman, M., & Martins, B. 2022, *MNRAS*, 514, 4803 7

Castro-Cisneros, J. D., Malhotra, R., & Rosengren, A. J. 2023, Communications Earth and Environment, 4, 372 3

Chambers, J. E. 1999, MNRAS, 304, 793 5

Chang, C.-K., Lin, H.-W., Ip, W.-H., et al. 2017, Geoscience Letters, 4, 17 2

Cheng, B., & Baoyin, H. 2024, Monthly Notices of the Royal Astronomical Society, 534, 1376 2

de la Fuente Marcos, C., & de la Fuente Marcos, R. 2016, MNRAS, 462, 3441 2, 4, 6

de la Fuente Marcos, C., & de la Fuente Marcos, R. 2025, Research Notes of the American Astronomical Society, 9, 235 2

Deo, S. N., & Kushvah, B. S. 2017, Astronomy and Computing, 20, 97 5

Farnocchia, D., Chesley, S. R., Vokrouhlický, D., et al. 2013, Icarus, 224, 1 7

Fenucci, M., & Novaković, B. 2021, AJ, 162, 227 2, 3, 4

Fenucci, M., Novaković, B., Zhang, P., et al. 2025, A&A, 695, A196 3

Folonier, H. A., Roig, F., & Beaugé, C. 2014, Celestial Mechanics and Dynamical Astronomy, 119, 1 9

Froeschlé, C., & Scholl, H. 1989, Celestial Mechanics and Dynamical Astronomy, 46, 231 3

Fujiwara, A., Kawaguchi, J., Yeomans, D. K., et al. 2006, Science, 312, 1330 11

Gladman, B. J., Migliorini, F., Morbidelli, A., et al. 1997, Science, 277, 197 3, 7

Glavin, D. P., Dworkin, J. P., Alexander, C. M. O., & et al. 2025, Nature Astronomy 11

Granvik, M., Morbidelli, A., Vokrouhlický, D., et al. 2017, A&A, 598, A52 11

Granvik, M., Morbidelli, A., Jedicke, R., et al. 2018, Icarus, 312, 181 3

Hamilton, V. E., Simon, A. A., Christensen, P. R., et al. 2019, Nature Astronomy, 3, 332 11

Hu, S., Li, B., Jiang, H., Bao, G., & Ji, J. 2023, AJ, 166, 178 2, 5

Huang, J., Ji, J., Ye, P., et al. 2013, Scientific Reports, 3, 3411 11

Jackson, J. 1913, MNRAS, 74, 62 2

Ji, J.-H., & Liu, L. 2007, ChJAA (Chin. J. Astron. Astrophys.), 7, 148 4

Jiang, Y., Ji, J., Huang, J., et al. 2015, Scientific Reports, 5, 16029 11

Jiao, Y., Cheng, B., Huang, Y., et al. 2024, Nature Astronomy, 8, 819 3, 11

Kitazato, K., Milliken, R. E., Iwata, T., & et al. 2019, Science, 364, 272 11

Lauretta, D. S., Balram-Knutson, S. S., Beshore, E., et al. 2017, Space Sci. Rev., 212, 925 11

Lauretta, D. S., Dellagiustina, D. N., Bennett, C. A., et al. 2019, Nature, 568, 55 11

Li, X., & Scheeres, D. J. 2021, Icarus, 357, 114249 2

Liu, L., Yan, J., Ye, M., et al. 2022, A&A, 667, A150 2, 4

Liu, L., Chen, Q., Yan, J., et al. 2024, Solar System Research, 58, 469 2

Michel, P., Morbidelli, A., & Bottke, W. F. 2005, Comptes Rendus Physique, 6, 291 3, 7

Mikkola, S., Innanen, K., Wiegert, P., Connors, M., & Brasser, R. 2006, MNRAS, 369, 15 2

Morais, M. H. M., & Morbidelli, A. 2002, Icarus, 160, 1 3

Morbidelli, A., Batygin, K., Brasser, R., & Raymond, S. N. 2020, MNRAS, 497, L46 4

Morbidelli, A., Bottke, Jr., W. F., Froeschlé, C., & Michel, P. 2002, in Asteroids III, ed. W. F. Bottke, Jr., A. Cellino, P. Paolicchi, & R. P. Binzel, 409 3, 11

Morbidelli, A., & Gladman, B. 1998, Meteoritics and Planetary Science, 33, 999, publisher: Wiley 9

Morbidelli, A., & Vokrouhlický, D. 2003, *Icarus*, 163, 120 3

Nesvorný, D. 2020, Nesvorný HCM Asteroid Families Bundle V1.0, NASA Planetary Data System, urn:nasa:pps:ast.nesvorný.families::1.0 4

Nesvorný, D., Deienno, R., Bottke, W. F., et al. 2023, *AJ*, 166, 55 4

Nesvorný, D., Vokrouhlický, D., Shelly, F., et al. 2024, *Icarus*, 417, 116110 4

Park, R. S., Folkner, W. M., Williams, J. G., & Boggs, D. H. 2021, *AJ*, 161, 105 5

Potiszil, C., Yamanaka, M., Ota, T., & et al. 2023, *Nature Communications*, 14, 6523 11

Pravec, P., & Harris, A. W. 2000, *Icarus*, 148, 12 2

Ren, J., Wu, B., Hesse, M. A., et al. 2024, *A&A*, 692, A62 2

Sharkey, B. N. L., Reddy, V., Malhotra, R., et al. 2021, *Communications Earth and Environment*, 2, 231 2, 3

Vokrouhlický, D., Bottke, W. F., Chesley, S. R., Scheeres, D. J., & Statler, T. S. 2015, arXiv preprint arXiv:1502.01249 5

Vokrouhlický, D., Bottke, W. F., & Nesvorný, D. 2017, *AJ*, 153, 172 4

Watanabe, S.-i., Tsuda, Y., Yoshikawa, M., et al. 2017, *Space Sci. Rev.*, 208, 3 11

Watanabe, S., Hirabayashi, M., Hirata, N., et al. 2019, *Science*, 364, 268 11

Wisdom, J. 1985, *Nature*, 315, 731 3

Yano, H., Kubota, T., Miyamoto, H., & et al. 2006, *Science*, 312, 1350 11

Ying, J., Ji, J., Jiang, H., et al. 2025, *Chinese Journal of Space Science*, 45, 736 2, 11

Zhang, P. F., Li, Y., Tang, J. Y., et al. 2025a, *Journal of Space Science and Experiment*, 2, 1 4

Zhang, P. F., Li, Y., Zhang, G. Z., et al. 2024, in LPI Contributions, Vol. 3040, 55th Lunar and Planetary Science Conference, 1845 2, 3, 4, 10

Zhang, R., Huang, J., He, R., Gen, Y., & Meng, L. 2019, *Journal of Deep Space Exploration*, 6, 417 11

Zhang, R., Zhang, H., Liu, J., et al. 2025b, *Scientia Sinica Physica, Mechanica & Astronomica*, 55, 279501 11

Zhou, L., Xu, Y.-B., Zhou, L.-Y., Dvorak, R., & Li, J. 2019, *A&A*, 622, A97 6

Zhou, Y. F., Li, H., Li, Z., & Zhou, L. 2024, *MNRAS*, 532, L7 11

Zhou, Y. F., Li, Z., Li, H., & Zhou, L. 2025, *MNRAS*, 538, 258 11

Zhu, M.-H., Morbidelli, A., Wei, Z., et al. 2025, *The Innovation*, publisher: Elsevier 3, 11